Understanding Improved Performance of Vacuum-Deposited All Small-Molecule Organic Solar Cells Upon Postprocessing Thermal Treatment

Suresh Madduri, Vaibhavi GKodange, Sai Santosh Kumar Raavi, and Shiv Govind Singh

***Abstract*—An all-inclusive investigation of the effect of postprocessing thermal treatment on all vacuum-deposited small-molecule organic solar cells (SM-OSC) is presented. Herein, DTDCTB is chosen as the donor (D) molecule, and three fullerene-derivative acceptor (A) molecules, namely, ICBA, C_{70}, and C_{60}, are chosen for the study, and the devices were optimized for PV. As the first step, OSC cells were fabricated and characterized for photophysical, morphology, as well as various photovoltaic parameters, such as V_{OC}, J_{SC}, FF, and η, and external quantum efficiency for different processing parameters, such as active layer concentration ratios and annealing temperatures. The devices based on ICBA were found to have outperformed the devices using C_{70} and C_{60}. OSC devices using ICBA as an acceptor are chosen for further characterization to establish the role of thermal treatment on their device performance. To this, 1-diode Shockley equation modeling is employed, and a qualitative relationship between diode saturation current and thermal annealing is obtained. Additionally, the charge recombination dynamics of the binary bulk heterojunction systems were investigated using the light intensity-dependent *J–V* characteristics, and the role of annealing in the reduction of trap-assistance recombination was established that corroborates well with the obtained annealing-dependent morphology information from AFM measurement.**

***Index Terms*—Annealing, morphology, organic solar cells (OSC), trap-assisted recombination.**

I. Introduction

UNDOUBTEDLY, the class of organic solar cells (OSC) with bulk heterojunction (BHJ) device structure has proven to be the most successful, owing to reduced exciton diffusion bottleneck and allowing the efficient exciton dissociation and charge transport leading to high power conversion efficiencies (PCE) [1], [2], [3], [4]. With the advent of nonfullerene acceptors, the record PCE of OSC has reached >18% [5], [6], [7], [8], [9]. To date, the most successful BHJ-OSC employ high-performance semiconducting polymers as donor systems and are typically solution processed [9], [10], [11]. Furthermore, the thermal postprocessing step has shown tremendous improvement in the polymer-based BHJ-OSC in terms of aiding favorable nanomorphology [12], [13]. In contrast, there is an inherent advantage with small-molecule donor molecules owing to their well-defined molecular structures, superior batch-to-batch reproducibility, and ease of thermal evaporation due to lower molecular weight, which has resulted in new attention toward the development of small-molecule organic solar cells (SM-OSC) [14], [15], [16], [17], [18], [19], [20], [21]. Following the success with polymer-based BHJ, most initial work on SM-OSC was devoted to solution-processed devices [22], [23], [24], [25], [26]. Remarkably, the low molecular weight of SMs can easily facilitate the deposition of an active layer via coevaporation of donor and acceptor molecules in a vacuum chamber [15], [16], [27], [28]. Few earlier reports demonstrated that coevaporation results in a homogenous blend, sometimes forbidding the formation of a suitable phase [29]. Thermal annealing cannot be expected to improve device performances as they tend to nucleate and crystallize postevaporation quickly on the target substrate instead of formation for efficient charge-percolation pathways [30], [31]. Yet, recent reports have proven otherwise with improved performances upon post-thermal treatment [15], [28], [32].

Overall, the field of vacuum-deposited SM-OSC is overlooked due to an unclear understanding of various mechanisms, many times leading to inferior performances and more so when fabricated using the thermal coevaporation method. Considering the growing need for scale-integrated device fabrication procedures, it is essential to address the issues abovementioned. In our recent brief report [15], we presented the role of annealing on the improved device performance via reduced trap-assisted recombination for small-molecule donor/acceptor blend consisting of DTDCTB as a donor [33], [34] and C_{70} as acceptor molecules. Herein, we present a comprehensive comparative study of the optimization and characterization of SM-OSC with DTDCTB as the donor and various fullerene derivatives, C_{60}, C_{70}, and

Manuscript received 27 July 2022; revised 19 October 2022; accepted 2 March 2023. Date of publication 22 March 2023; date of current version 20 April 2023. The work of V. G. Kodange was supported by DST-INSPIRE under Grant IF190222. The work of S. S. K. Raavi was supported in part by Project BRICS/PilotCall2/IEEE-OSC/2018 (G), Project CRG/2019/003197, and Project TMD/SERI/S81. The work of S. G. Singh was supported by DST_FIST. *(Corresponding author: Shiv Govind Singh.)*

Suresh Madduri and Shiv Govind Singh are with the Department of Electrical Engineering, Indian Institute of Technology Hyderabad, Kandi, Sangareddy, Telangana 502285, India (e-mail: ee17resch01005@iith.ac.in; sgsingh@iith.ac.in).

Vaibhavi GKodange is with Department of Physics, Indian Institute of Technology Hyderabad, Kandi, Sangareddy Telangana 502285, India (e-mail: ph20resch01003iith.ac.in).

Sai Santosh Kumar Raavi is with Department of Physics, Indian Institute of Technology Hyderabad, Kandi, Sangareddy, Telangana 502285, India, and also with the Department of Climate Change, Indian Institute of Technology Hyderabad, Kandi, Sangareddy, Telangana 502285, India (e-mail: sskraavi@phy.iith.ac.in).

This article has supplementary material provided by the authors and color versions of one or more figures available at https://doi.org/10.1109/JPHOTOV.2023.3254307.

Digital Object Identifier 10.1109/JPHOTOV.2023.3254307

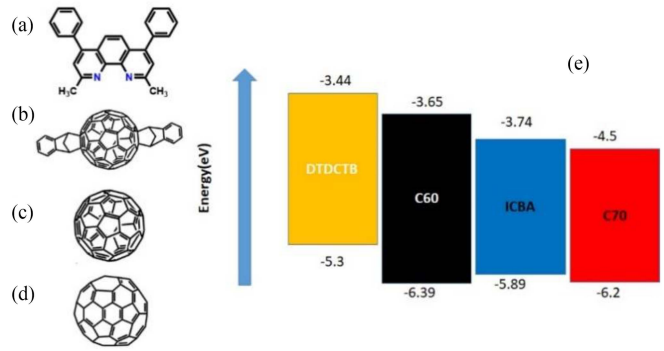

Fig. 1. Chemical structures of (a) DTDCTB, (b) ICBA, (c) C60, and (d) C70. (e) Energy level diagram.

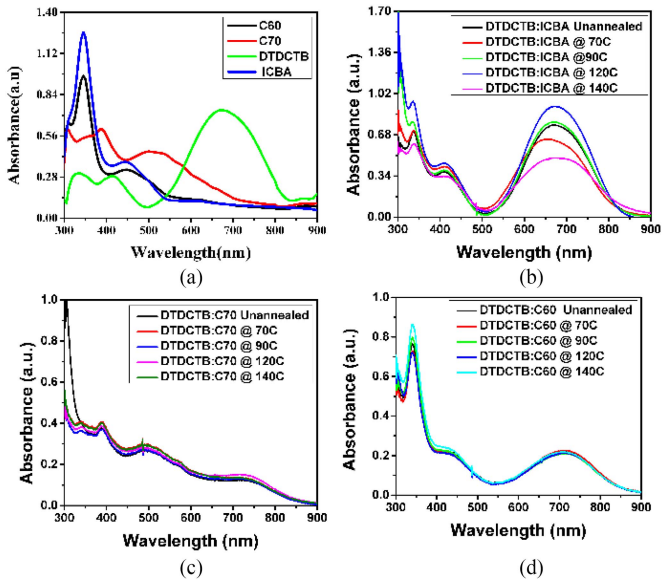

Fig. 2. (a) UV-Visible absorption spectra of neat DTDCTB, ICBA, C60, and C70 thin films. (b) and (c) UV-Visible absorption spectra of binary blend films.

ICBA, as acceptor systems. At the outset, we establish the optimal annealing temperature for two active layer thicknesses and obtain the best-performing devices with an efficiency of ≈ 3.2% for DTDCTB:ICBA at 90 °C specific to the device area considered in the study. The focus of the study presented here is primarily aimed at understanding the effect of thermal treatment on morphology and various photovoltaic parameters, such as external quantum efficiency (EQE), short-circuit current density (J_{SC}), and open-circuit voltage (V_{OC}), and correlating with the charge recombination process with additional information obtained from photoluminescence (PL) spectroscopy. Notably, the devices with ICBA performed better than C_{70} and C_{60}, unlike what is observed in the case of polymer-based devices, where reduced PCE of OSC employing fullerene multiadducts as acceptors were used [35]. Recently, Yue et al. [36] reported vacuum-deposited OSCs utilizing a low-bandgap nonfullerene acceptor (CBD) and DTDCTB as the donor, with an efficiency of 0.86% obtained with a planar architecture. Therefore, one can surmise that the efforts toward developing vacuum-deposited SM-OSCs are still nascent. The results presented in this report are expected to lead to future innovations.

II. Experimental Details

A. Device Fabrication

Patterned ITO-coated glass substrates used in this study were procured from Ossilla, Ltd. High-purity DTDCTB (2-[[7-[5-[Bis(4-methylphenyl) amino]-2-thienyl]-21,3-benzothiadiazol-4-yl] methylene] propanedinitrile), ICBA (1′,1″,4′,4″-Tetrahydro-di [1], [4] methanonaphthaleno [12:2′,3′,56,60:2″,3″] [5], [6] fullerene-C_{60}), C_{70}, and C_{60} are purchased from Sigma Aldrich and used without further purification. DTDCTB is an electron donor material and C_{60}, C_{70}, and ICBA materials are used as electron acceptor materials. MoO_3 and bathocuprione (BCP) materials are used as hole transport layer (HTL) and electron transport layers, respectively. Conventional architecture solar cells devices' with structures ITO/MoO_3 (20 nm)/DTDCTB:Acceptor/BCP(10 nm)/Ag(100 nm) were fabricated using the vacuum-based thermal evaporation technique and sputtering techniques (integrated with the Jacomex glove box with controlled conditions). All the thin films are deposited with base pressure of 5×10^{-6} mbar. The active layer codeposition was performed at a rate of 1–1.5 Å/s, whereas metal and transport layers were performed at a rate of 0.5–1 Å/s. The substrate was kept at room temperature. Thicknesses were optimized by a profilometer, and the layer-by-layer thicknesses were monitored using crystal thickness monitors during the deposition. The active area of the devices was 0.045 cm^2. Post-thermal treatment at 70, 90, 120, and 140 °C was performed by using hot plate inserted into the glovebox to maintain annealing in the controlled conditions.

B. Characterization

The obtained blends on ITO substrates are characterized for changes in absorption using FR-Basic UV/VIS absorption spectrometer, and the morphology changes before and after annealing are imaged using atomic force microscopy (AFM, Bruker). The $J-V$ characteristics of the fabricated devices are performed using a class AAA solar simulator (ScienceTech, Inc.). Intensity-dependent measurements are achieved by varying the distance between the device and solar lamp and characterizing the intensity with a standard Si solar cell. The PL spectroscopy investigations are performed using the FLS1000 spectrometer (Edinburg Instruments). Fig. 1 shows the donor and acceptors' chemical structures and HOMO/LUMO energy levels.

III. Results and Discussion

A. Photophysical Investigations

The wavelength absorption spectra of individual thin films DTDCTB, ICBA, C_{60}, C_{70}, and BHJ thin films DTDCTB:ICBA, DTDCTB:C_{60}, and DTDCTB:C_{70} are shown in Fig. 2. The absorption spectrum of DTDCTB film is dominant from 500 to 820 nm, extending from the visible to the near-IR spectral region. The highest absorption peaks in the DTDCTB thin film

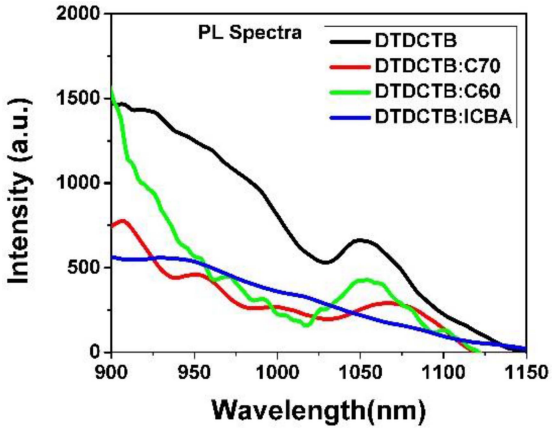

Fig. 3. Steady-state NIR fluorescence spectra of DTDCTB, DTDCTB:ICBA, DTDCTB:C_{70}, and DTDCTB:C_{60} binary BHJ blends annealed at 90 °C, excited at 600 nm.

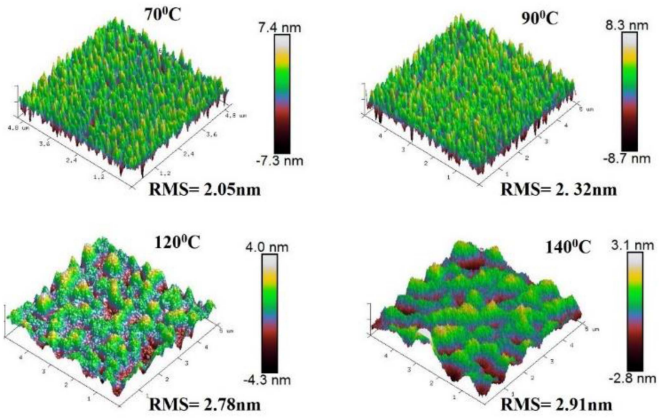

Fig. 4. AFM topography images (5 μm × 5 μm) of blend films DTDCTB: ICBA (1:1.2) with different annealing temperatures.

TABLE I
PL QUENCHING EFFICIENCY VALUES OF BLENDS, PCE VALUES OF THE BINARY BHJ SOLAR CELLS WITH 1:1.2 RATIOS, ANNEALED AT 90 °C, AND EMISSION MAXIMA IN NIR WHEN EXCITED AT 600 NM

Blends(90°C)/parameters	DTDCTB: ICBA	DTDCTB:C_{60}	DTDCTB:C_{70}
PCE (%)	3.12 ±0.2	2.7 ±0.1	2.8 ±0.3
PL Quenching efficiency (%)	55.85	39.58	32.90
Emission maxima in NIR	~900 nm	~900 nm, 1050 nm	~900 nm, 1050 nm

are observed at 330 nm, 417 nm, and 672 nm, respectively. Similarly, the absorption spectrum of C_{60}, C_{70}, and ICBA thin film is from 300 to 520 nm. Once these materials are codeposited, the pan-chromatic absorption of the active layer leads to efficient light harvesting. Fig. 2(b) and (c) shows that as the annealing temperature increases (70 °C, 90 °C, 120 °C, and 140 °C), there is a slight increment in absorption intensity at each annealing temperature and found that the optimum annealing temperature was at 90 °C. This increase may be due to the reduction in Columbic force of attraction in the excitons and, hence, creating free electron−hole $(e - h)$ pairs in the device [25], [28].

PL emission of the blends DTDCTB:ICBA, DTDCTB:C_{60}, and DTDCTB:C_{70} was measured using the Edinburg FLS1000 PL spectrometer. Thin films of 70 nm were deposited by thermal evaporation on glass substrates at 1:1.2 concentration ratio and annealed at 90 °C, for which the best PCE for the corresponding devices was obtained. The peaks and quenching were qualitatively studied. Quantitative calculations of quenching efficiency from the fluorescence spectra for DTDCTB (donor) and the blends with each acceptor to understand the effect of charge transfer and in turn on the PCE of the corresponding OPV devices.

Fig. 3 illustrates the NIR emission spectra of pure DTDCTB thin film and blends of this DTDCBT with ICBA, C_{60}, C_{70} excited at 600 nm, and the corresponding emission maxima, as well as quenching efficiencies, are presented in Table I. The peak around 900 nm corresponds to S_1 to S_O electronic transition [37]. DTDCTB:C_{70} are similar except for the quenching, including the small peak around 1050 nm. On the other hand, the extent of quenching is higher for DTDCTB:ICBA blend with respect to the donor, and the 1050 nm peak has disappeared in the blend. This indicates charge transfer at the donor–acceptor interface after exciton dissociation, where the final state involves electron in the acceptor and hole in the donor. This reduces the possibility of radiative deactivation that can occur via geminate recombination, which can be one of the reasons for quenching in the blend emission [20], [38]. The quenching efficiencies can be roughly correlated with the PCE values of the corresponding devices. Out of the three, DTDCTB:ICBA blend shows the maximum quenching efficiency and, hence, expected to exhibit the best device PCE.

The post-thermal treatment affects the quenching as the nanomorphology of D/A interface varies, resulting in better charge transfer efficiency that manifests as higher PL quenching. Evidently from Fig. 3, a better quenching is observed for DTDCTB:ICBA blend that corroborates with better PCE compared to devices employing C_{70} and C_{60} acceptors. However, it should be noted that several other factors are also responsible for the PL quenching, and hence, these are not directly correlated in this work. Generally, the additional quenching mechanisms involved are energy transfer (where the excess energy due to a relaxing donor chromophore is nonradiatively transported to the acceptor molecule), collisional quenching (where nonradiative transitions are facilitated by collision of excited fluorophore with another molecule such as O_2), static quenching (when a ground state complex is formed with another molecule), etc. [39]. Energy transfer requires the spectral overlap of donor emission with acceptor absorption, which is clearly not the case at 600 nm excitation [see Figs. 2(a) and 3], and hence, this option can be eliminated [37], [39].

B. Morphology Characterization

AFM topographical 3-D images of the DTDCTB:ICBA blend films of 1:1.2 and 1:1.5 are depicted in Figs. 4 and 5, respectively. The morphological studies of blend films clarify the influence of thermal annealing. The thin films were prepared by thermal evaporator (coevaporation) on glass substrates. The prepared

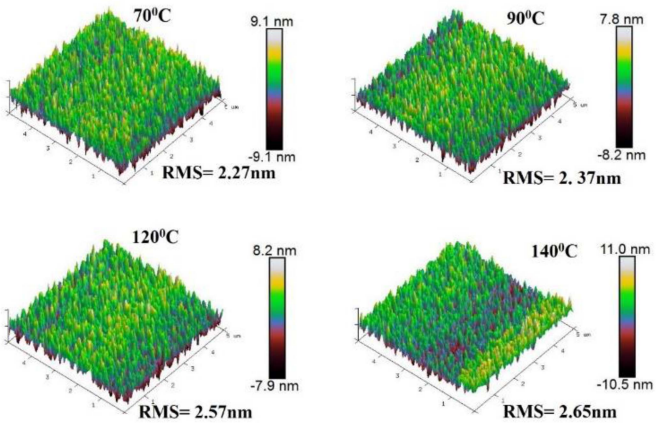

Fig. 5. AFM topography images (5 μm $\times$ 5 μm) of blend films DTDCTB:ICBA (1:1.5) with different annealing temperatures.

thin films were annealed at various temperatures on a hot plate, and we observed the DTDCTB:ICBA blend film's top surface by using AFM in the tapping mode. At the thermal annealing temperatures at 70 and 90 °C, there is not much variation in the film morphology, whereas at ≥120 °C, there are significant changes in the surface morphology. Excess thermal annealing (≥120 °C) increased the domain sizes, which is unfavorable for efficient exciton dissociation charge extraction through interpenetrating networks of the two phases [13], [25], [26], [28], [40]. The morphology images of blends with C_{70} and C_{60} are shown in Figs. S1 and S2 (see Supplementary Information). The trend of RMS roughness from 70 °C annealing temperature to 90 °C annealing temperature is minimal (i.e., increase in RMS roughness is 13% in the case of DTDCTB:ICBA 1:1.2 while 4% RMS roughness increment in the case of 1:1.5). Similarly, the same trend has been observed in the devices in Table II. However, upon further increase in annealing temperature increases the RMS roughness and, due to this, increases the domain sizes, which is unfavorable for efficient exciton dissociation charge extraction through interpenetrating networks of the two phases [28]; eventually, it reduces the PCE of the fabricated solar cells.

TABLE II
VARIOUS PARAMETERS OF THE BINARY BHJ SOLAR CELLS WITH 1:1.2 AND 1:1.5 (D:A) RATIOS

Annealing temperature/parameters	V_{oc}(V)	J_{sc}(mA/cm^2)	FF (%)	PCE (%)
DTDCTB:C60 (1:1.2) 70 °C	0.72 ±0.06	-9.44 ±0.4	38.5 ±5.5	2.63 ±0.5
90 °C	**0.74 ±0.01**	**-8.9±0.09**	**41.1 ±1.6**	**2.7±0.1**
120 °C	0.335 ±0.04	-8.05 ±0.3	33.6 ±1.6	0.91 ±0.1
140 °C	0.46 ±0.05	-8.1 ±0.1	33.6 ±3.05	1.2 ±0.2
DTDCTB:C70 (1:1.2) 70 °C	0.71 ±0.03	-6.7±0.4	33.9 ±1.9	1.6 ±0.2
90 °C	**0.72±0.03**	**-10.4 ±0.8**	**37.7 ±2.3**	**2.8 ±0.3**
120 °C	0.71 ±0.02	-9.01±0.4	43.6±4.4	2.8 ±0.4
140 °C	0.56 ±0.04	-7.2±0.84	34.5 ±3.4	1.4 ±0.39
DTDCTB: ICBA (1:1.2) 70 °C	0.71 ±0.1	-10.6 ±0.2	40.07 ±1.8	3.05 ±0.1
90 °C	**0.72 ±0.1**	**-9.9 ±0.6**	**43.4 ±0.2**	**3.12 ±0.2**
120 °C	0.48 ±0.01	-9.1 ±0.1	38.2 ±6.6	1.70 ±0.2
140 °C	0.33 ±0.01	-8.7 ±0.1	40.9 ±0.6	1.18 ±0.02
DTDCTB: ICBA (1:1.5) 70 °C	0.68 ±0.1	-8.13 ±0.9	37.03 ±11.4	2.18 ±1.3
90 °C	**0.69 ±0.14**	**-9.02 ±0.49**	**37.08 ±15.3**	**2.45 ±1.5**
120 °C	0.52 ±0.03	-5.26 ±1.5	42.65±0.72	1.19 ±0.4
140 °C	0.22 ±0.02	-7.24 ±0.4	41.8 ±8.4	0.68 ±0.2

Standard deviation of six devices with 95% confidence value and the margin of error mentioned in brackets.

C. J–V and EQE Investigations

Optimizing the annealing temperature and concentration ratios had to be performed to see the effect of thermal annealing temperature on the fabricated solar cell devices. The $J-V$ characteristics of the fabricated solar cell devices (ITO/MoO_3/DTDCTB:C_{60}/BCP/Ag, ITO/MoO_3/DTDCTB:C_{70}/BCP/Ag, and ITO/MoO_3/DTDCTB: ICBA/BCP/Ag) with different annealing temperatures under 1-sun illumination are presented in Fig. 6, and the various photovoltaic parameters are summarized in Table II.

Initially, an optimal thermal annealing temperature was found by annealing the devices for 30 min at various annealing temperatures (70 °C, 90 °C, 120 °C, and 140 °C, respectively) and subsequently found the optimal annealing temperature, i.e., 90 °C. As the annealing temperature increases, V_{OC}, J_{SC}, and FF are also increased and reached to a maximum value at 90 °C. At 90 °C, for DTDCTB:C_{60}(1:1.2 ratio), we have achieved V_{OC} of 0.74 V, J_{SC} of -8.91 mA/cm^2, FF of 42.7%, and PCE (η) of 2.8%. Similarly, for DTDCTB:C_{70} (1:1.2) ratio, we have achieved V_{OC} of 0.72 V, J_{SC} of -11.2 mA/cm^2, FF of 40%, and η of 3.1%, respectively. And also, in the case of DTDCTB:ICBA at 90 °C, annealing obtained η of 3.32% with V_{OC} of 0.73 V, J_{SC} of -10.5 mA/cm^2, and maximum FF of 43.6%. This could be due to more ordered donor/acceptor domains with efficient packing that might be formed, and hence, it is beneficial for the charge transport in the devices. However, further increase in annealing temperature (i.e., ≥120 °C) leads to the degradation of the device performance due to unfavorable coarsening of the acceptor and donor domains and formation of larger donor/acceptor domain sizes leading to the recombination of electron and hole pairs within the devices. The variation in the series and shunt resistances of the unannealed and annealed

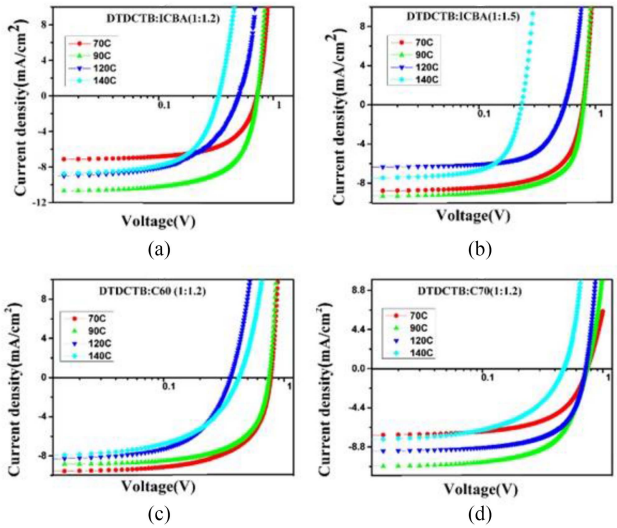

Fig. 6. *J–V* curves of the binary BHJ solar cells fabricated in this study.

devices at 90 °C is tabulated in Table S1 (see Supplementary Information).

The EQE spectra of the devices (1:1.5 and 1:1.2 ratios) with various annealing temperatures were recorded and displayed in Fig. 7. It shows the photoresponse over the broad spectrum from 300 to 850 nm. Notably, at optimum annealing temperature, the devices gave higher EQE values over the whole spectral response range, which is accounted for enhancement in photocurrents with the increased annealing temperature and reached maximum at 90 °C.

D. Effect of Thermal Annealing on V_{OC}

Considering the devices with ICBA that exhibited better performance, a detailed analysis of role of thermal annealing is presented subsequently. In order to investigate the effect of thermal annealing on V_{OC}, the best performance $J-V$ curves of DTDCTB:ICBA devices at different annealing temperatures have to be considered by using the 1-diode Shockley equation [41], [42]. From this equation, we can clearly study the $J-V$ behavior of solar cell devices [26], [43], [44], [45]. The Shockley equation for describing the current density (J) versus voltage (V) characteristics of the OSC is given by

$$J\left(\mathrm{V}\right)=J_0\left\{\left[e^{\frac{q(V-JRs)}{\eta K_b T}}\right]-1\right\}+\frac{V-J_{Rs}}{R\mathrm{sh}}-J_{\mathrm{ph}}\left(\mathrm{V}\right). \quad (1)$$

From (1), $J(\mathrm{V})$ is the solar cell output current, J_0 is the reverse saturation current density, q is the electron charge, T is the absolute temperature, η is the ideality factor, R_S is the series resistance of the solar cell device, R_{Sh} is the shunt resistance of the device, and J_{Ph} is the voltage-dependent photocurrent density. At the open-circuit condition, $J=0$, $V=V_{\mathrm{OC}}$. Assuming R_S is low and R_{Sh} is high, (1) can be simplified and further solved for obtaining the equation for V_{OC}

$$V_{\mathrm{OC}}=\frac{\eta kT}{q}\ln\left(\frac{J_{\mathrm{ph}}\left(V_{\mathrm{OC}}\right)}{J_0}\right). \quad (2)$$

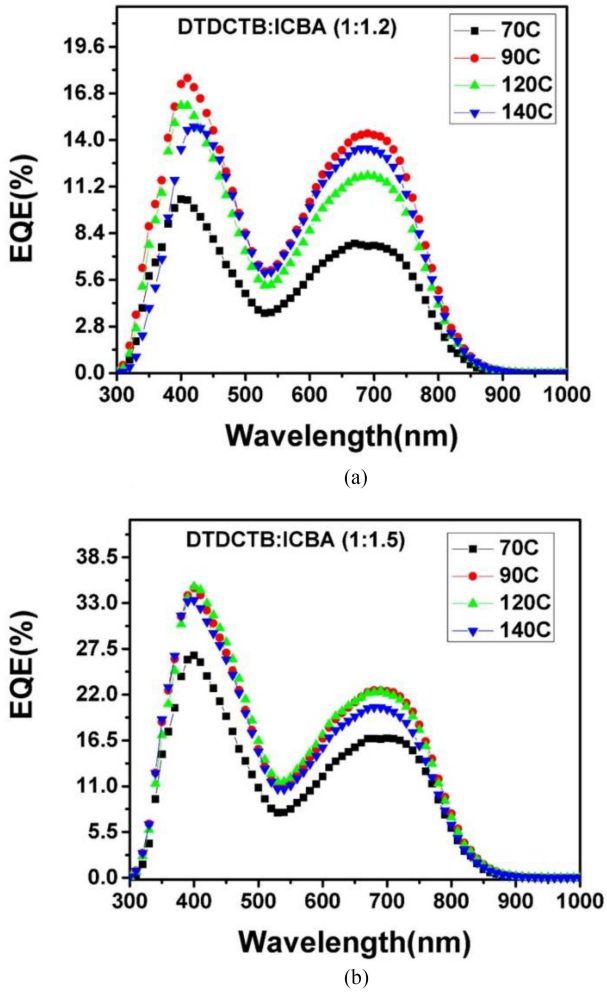

Fig. 7. EQE curves of DTDCTB:ICBA with 1:1.5 and 1:1.2 (D:A) devices.

In (2), J_{Ph} (V_{OC}) is the photocurrent density at $V=V_{\mathrm{OC}}$ and is equivalent to the dark current density at V_{OC}. At dark conditions, J_{Ph} (V) $=0$, and assuming R_S is low and R_{Sh} is high, the equation can be rewritten as

$$J\left(V\right)=J_0\left\{\exp\left(\frac{qV}{\eta kT}\right)-1\right\}. \quad (3)$$

$J-V$ dark data of the best devices with different annealing temperatures were considered and fitted in (3) by using origin software and hence the extracted J_0 and η are summarized in Table III. By substituting J_0, η, and J_{Ph} (V_{OC}) into (1), we calculated the open-circuit voltages at the respected annealing temperatures. From Table III, we can notice that as the annealing temperature increases, the values of J_0, η, and calculated V_{OC} decreased. From (2), the calculated V_{OC} values decrease with the annealing temperatures and this is due to J_0, which is inversely proportional to V_{OC} [from (2)]. The same trends were observed with devices with ratios of D:A of 1:1.2 and 1:1.5 [46], [47], [48].

J_{ph} versus V_{eff}: Fig. 8 depicts the photocurrent density (J_{Ph}) versus effective voltage (V_{eff}) for the devices (DTDCTB:ICBA, 1:1.2 and 1:1.5 ratios) at different annealing temperatures. These

TABLE III
SUMMARY OF EXTRACTED PARAMETERS FROM $J-V$ AND $J_{PH}-V$ CURVES OF 1:1.2 AND 1:1.5 (DTDCTB:ICBA) BLENDS WITH VARIOUS ANNEALING TEMPERATURES

D/A	Annealing temperature	Ideality factor (η)	J_0	$J_{ph}(V_{oc})$ [mA/cm^2)]	V_{oc} cal (V)	V_{oc}(V)
1:1.2	70 °C	1.27	2.34×10^{-8}	0.5	0.63	0.72
	90 °C	1.14	1×10^{-7}	1.17	0.58	0.73
	120 °C	0.98	7.42×10^{-7}	0.23	0.43	0.49
	140 °C	0.86	1.76×10^{-5}	0.37	0.29	0.33
1:1.5	70 °C	1.13	4.37×10^{-8}	1.37	0.63	0.78
	90 °C	1.15	3.19×10^{-8}	0.641	0.62	0.79
	120 °C	1.10	7.86×10^{-6}	2.43	0.50	0.54
	140 °C	0.47	8.37×10^{-4}	1.01	0.14	0.23

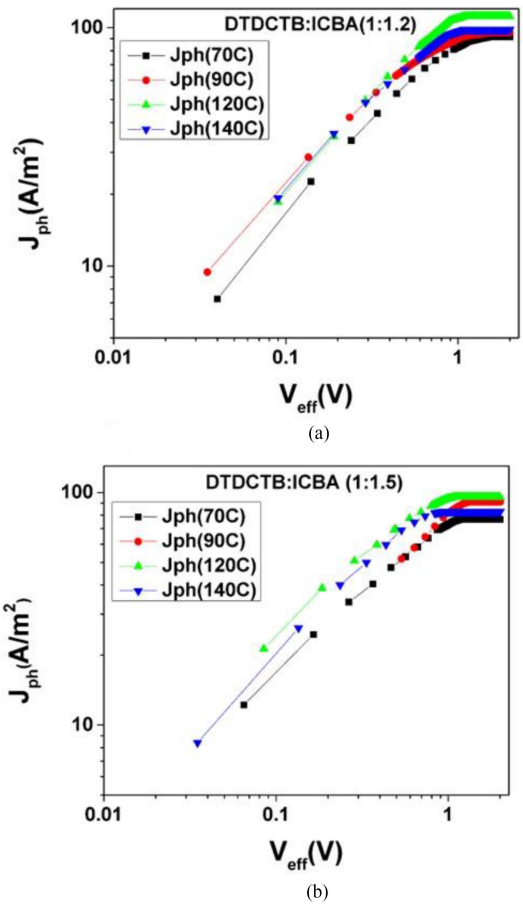

Fig. 8. Photocurrent density and effective voltage curves for DTDCTB:ICBA binary blend of two concentration ratios 1:1.2 and 1:1.5.

characteristics give more insight on exciton generation and dissociation processes by determining the photocurrent saturation densities (J_{Ph}) [49], [50], [51], [52].

The J_{Ph} is determined by $J_{Ph} = J_L - J_D$, where J_L and J_D are current densities under light and in the dark conditions, respectively, and $V_{eff} = V_0 - V_A$, where V_A is the applied bias voltage and V_0 is the voltage at which J_{Ph} is 0 (i.e., $J_L = J_D$). J_{Ph} is linearly increased at lower values of V_{eff} and then saturated at suffiently high values of V_{eff}. In general, it is assumed that all the generated photoexcitons are dissociated at the D/A interface into free charge carriers at higher V_{eff}. These free electrons are contributed to the current under saturation region due to sufficient electric field and obtained the maximum generation rate (G_{max}) by the equation, $J_{sat} = qG_{max}\ L$, where 'q' is the electron charge, L is the active layer thickness, and G_{max} is the maximum generation rate. The obtained G_{max}values are tabulated in Table IV.

TABLE IV
SUMMARY OF EXTRACTED PARAMETERS (J_{PH}, J_{SAT}, G_{MAX}) AND DISSOCIATION PROBABILITIES P (E, T)

D/A	Annealing temperature	Jph(mA/cm^2)	J_{sat} (A/cm^2)	Gmax(m^{-3}s^{-1})	J_{ph}/J_{sat}
1:1.2	70 °C	71.6	84.42	7.53×10^{27}	84.81%
	90 °C	107.4	124.45	11.11×10^{27}	86.29%
	120 °C	91.4	125.17	11.1×10^{27}	73.12%
	140 °C	88.5	124.27	11.09×10^{27}	71.21%
1:1.5	70 °C	88.3	102.84	9.18×10^{27}	85.86%
	90 °C	93.6	108.12	9.65×10^{27}	86.57%
	120 °C	64	77.45	6.9×10^{27}	82.63%
	140 °C	75.4	104.17	9.3×10^{27}	72.38%

Further, the exciton dissociation probability of the devices is estimated. In any OSC, only a fraction of the photogenerated excitons can be dissociated and others may recombine. Therefore, J_{Ph} can be determined by $J_{Ph} = qG_{max}\ P(E,T)L$, where $P(E,T)$ is the dissociation probability of the device which is the function of electric field (E) and temperature (T). The quantity $P(E,\ T)$ can be determined from the ratio of J_{Ph}/J_{sat}. The obtained $P(E,\ T)$ are tabulated in Table IV. In summary, when the annealing temperature increased, J_{Ph} and G_{max} are also increased and reached to a maximum value and then it got reduced, and the dissociation probabilities are maximum at the optimum annealing temperature, i.e., at 90 °C. The dissociation probabilities of 1:1.2 and 1:1.5 (D: A) devices are 86.29% and 86.57%, respectively.

E. Dependence of Light Intensity on Charge Recombination Dynamics

The quantities and V_{OC} at various light intensities offer the deeper insight on recombinations present in the system [20], [26], [51], [52]. In principle, J_{SC} follows the power law dependence with respect to the light intensity (P_{in}) in an OSC device as $J_{SC} \propto (P_{in})^{\alpha}$. Fig. 9(a) displays J_{SC} as a function of light intensities in the double logarithmic scale. From the obtained J_{SC} data, we extracted the exponent (α) values and they are 1.25, 1.15, 1.18, and 1.14, respectively, and it is close to the ideal value (unity). The α values are close to 1 and have minor variation, which is indicating that there are no weak bimolecular recombinations and space charge effects in the device. Fig. 9(b) shows the relationship between V_{OC} and illumination light intensities of BHJ solar cell device. The slope of V_{OC} versus $\log(P_{in})$ determines the trap-assisted recombinations

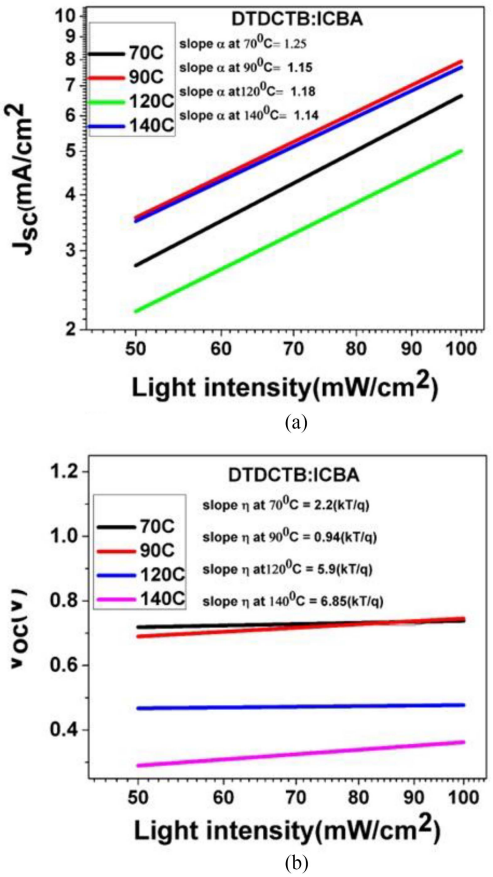

Fig. 9. (a) Dependence of $J_{\rm sc}$ on light intensity. (b) Dependence of $V_{\rm OC}$ on light intensities of DTDCTB:ICBA BHJ systems.

present in the BHJ OSC. In general, $V_{\rm OC} = \frac{kT}{q}\log(P_{\rm in})$, where k is Boltzmann's constant, T is the temperature, and 'q' is the electron charge. The slope of $\frac{kT}{q}$ implies that the bimolecular recombination is a dominant mechanism within the device; if the slope is greater than $\frac{kT}{q}$, then it indicates that a trap-assisted or SRH recombination may be present in the device. From Fig. 9, we extracted the slope values, i.e., $2.2(\frac{kT}{q})$ and $0.94(\frac{kT}{q})$, $5.94(\frac{kT}{q})$ and $6.85(\frac{kT}{q})$, respectively, and denote that there is trap-assisted recombinations within the device at all annealing temperatures except 90 °C. Similar measurements performed for DTDCTB:C_{60} and DTDCTB:C_{70} BHJ systems are presented in Fig. S3 (see Supplementary Information). Evidently, the devices consisting of blend with ICBA outperforms those with the other blends.

IV. Conclusion

In this article, a comprehensive analysis on the understanding of post-thermal treatment on vacuum-deposited SM-OSC is presented. To this, we have fabricated thermally evaporated small-molecule-based DTDCTB:ICBA, DTDCTB:C60, and DTDCTB:C70 binary BHJ solar cells and thoroughly investigated the influence of thermal annealing at different temperatures on these devices. From $J-V$ curve analysis, as the annealing temperature increases, $V_{\rm OC}$, $J_{\rm SC}$, FF, and η increased and reached at maximum value at optimum annealing temperature at 90 °C and then reduced all the device parameters drastically. Meanwhile, morphological studies suggest that at higher annealing temperatures ($\geq$120 °C), the phase sizes (donor/acceptor domain sizes) are increased and resulted in recombination within the device. A qualitative relationship was established between the diode saturation current and thermal annealing, which gives a clear view of studying SM-OSC with the diode current equations and extracted all the parameters related to them. $J_{\rm Ph}$ versus $V_{\rm eff}$ curves suggested the charge carrier generation rates and dissociation probabilities information clearly. Light-dependent studies strongly suggest that the devices are dominating with trap-assisted recombination while bimolecular recombination are reduced. Therefore, this investigation provides detailed information for annealing-dependent studies of thermally evaporated BHJ OSC and will also be useful in device optimization for higher performance small-molecule-based OPV cells.

References

[1] S. H. Park et al., "Bulk heterojunction solar cells with internal quantum efficiency approaching 100%," *Nature Photon.*, vol. 3, no. 5, pp. 297–303, 2009.
[2] M. Jørgensen et al., "Stability of polymer solar cells," *Adv. Mater.*, vol. 24, no. 5, pp. 580–612, 2012.
[3] G. Zhang et al., "Nonfullerene acceptor molecules for bulk heterojunction organic solar cells," *Chem. Rev.*, vol. 118, no. 7, pp. 3447–3507, 2018.
[4] Y. Huang, E. J. Kramer, A. J. Heeger, and G. C. Bazan, "Bulk heterojunction solar cells: Morphology and performance relationships," *Chem. Rev.*, vol. 114, no. 14, pp. 7006–7043, 2014.
[5] K. Jin, Z. Xiao, and L. Ding, "18.69% PCE from organic solar cells," *J. Semicond.*, vol. 42, no. 6, pp. 2020–2022, 2021.
[6] M. Zhang et al., "Single-layered organic photovoltaics with double cascading charge transport pathways: 18% efficiencies," *Nature Commun.*, vol. 12, no. 1, pp. 1–10, 2021.
[7] Y. Lin et al., "18.4% organic solar cells using a high ionization energy self-assembled monolayer as hole-extraction interlayer," *ChemSusChem*, vol. 14, no. 17, pp. 3569–3578, 2021.
[8] Y. Cui et al., "Single-junction organic photovoltaic cell with 19% efficiency," *Adv. Mater.*, vol. 33, no. 41, pp. 1–8, 2021.
[9] Y. Cui et al., "Single-junction organic photovoltaic cells with approaching 18% efficiency," *Adv. Mater.*, vol. 32, no. 19, pp. 1–7, 2020.
[10] A. J. Heeger, "Semiconducting polymers: The third generation," *Chem. Soc. Rev.*, vol. 39, no. 7, pp. 2354–2371, 2010.
[11] M. Zhang, X. Guo, W. Ma, H. Ade, and J. Hou, "A large-bandgap conjugated polymer for versatile photovoltaic applications with high performance," *Adv. Mater.*, vol. 27, no. 31, pp. 4655–4660, 2015.
[12] H. Hoppe and N. S. Sariciftci, "Morphology of polymer/fullerene bulk heterojunction solar cells," *J. Mater. Chem.*, vol. 16, no. 1, pp. 45–61, 2006.
[13] E. Verploegen et al., "Effects of thermal annealing upon the morphology of polymer-fullerene blends," *Adv. Funct. Mater.*, vol. 20, no. 20, pp. 3519–3529, 2010.
[14] A. Venkateswararao and K. T. Wong, "Small molecules for vacuum-processed organic photovoltaics: Past, current status, and prospect," *Bull. Chem. Soc. Jpn.*, vol. 94, no. 3, pp. 812–838, 2021.
[15] S. Madduri, V. S. Katta, S. S. K. Raavi, and S. G. Singh, "Annealing induced control of trap-assisted recombination in vacuum-deposited small-molecule solar cells," *Mater. Lett.*, vol. 300, 2021, Art. no. 130159.
[16] D. Park, I. H. Jung, S. Y. Jang, and S. Yim, "Vacuum-deposited organic solar cells based on a dicyanovinyl-terminated small-molecule donor," *Macromol. Res.*, vol. 27, no. 5, pp. 444–447, 2019.
[17] S. D. Collins, N. A. Ran, M. C. Heiber, and T. Q. Nguyen, "Small is powerful: Recent progress in solution-processed small molecule solar cells," *Adv. Energy Mater.*, vol. 7, no. 10, 2017.
[18] G. Chen et al., "Comparison of the solution and vacuum-processed squaraine: Fullerene small-molecule bulk heterojunction solar cells," *Front. Chem.*, vol. 6, pp. 1–9, 2018.

[19] Y. Lin, Y. Li, and X. Zhan, "Small molecule semiconductors for high-efficiency organic photovoltaics," *Chem. Soc. Rev.*, vol. 41, no. 11, pp. 4245–4272, 2012.
[20] S. Madduri, V. G. Kodange, S. S. K. Raavi, and S. G. Singh, "Optimization of thermally evaporated small molecule ternary organic solar cells," in *Proc. IEEE 48th Photovoltaic Spec. Conf.*, 2021, pp. 732–736.
[21] A. Mishra et al., "A-D-A-type S,N-Heteropentacenes: Next-generation molecular donor materials for efficient vacuum-processed organic solar cells," *Adv. Mater.*, vol. 26, no. 42, pp. 7217–7223, 2014.
[22] D. Hu et al., "15.34% efficiency all-small-molecule organic solar cells with an improved fill factor enabled by a fullerene additive," *Energy Environ. Sci.*, vol. 13, no. 7, pp. 2134–2141, 2020.
[23] Z. Kan et al., "Triple bulk heterojunctions as means for recovering the microstructure of photoactive layers in organic solar cell devices," *Sol. Energy Mater. Sol. Cells*, vol. 120, pp. 37–47, Jan. 2014.
[24] B. Walker et al., "Nanoscale phase separation and high photovoltaic efficiency in solution-processed, small-molecule bulk heterojunction solar cells," *Adv. Funct. Mater.*, vol. 19, no. 19, pp. 3063–3069, 2009.
[25] X. Wan et al., "Improved efficiency of solution processed small molecules organic solar cells using thermal annealing," *Org. Electron.*, vol. 14, no. 6, pp. 1562–1569, 2013.
[26] Z. Yi et al., "Effect of thermal annealing on active layer morphology and performance for small molecule bulk heterojunction organic solar cells," *J. Mater. Chem. C*, vol. 2, no. 35, pp. 7247–7255, 2014.
[27] A. Mishra and P. Bäuerle, "Vacuum-processed donor materials for organic photovoltaics," *Organic Photovoltaics: Materials, Device Physics, and Manufacturing Technologies*, 2nd ed. Hoboken, NJ, USA: Wiley, 2014, pp. 139–170, 2014.
[28] P. Kovacik, H. E. Assender, and A. A. R. Watt, "Morphology control in co-evaporated bulk heterojunction solar cells," *Sol. Energy Mater. Sol. Cells*, vol. 117, pp. 22–28, 2013.
[29] J. Xue, B. P. Rand, S. Uchida, and S. R. Forrest, "Mixed donor-acceptor molecular heterojunctions for photovoltaic applications. II. Device performance," *J. Appl. Phys.*, vol. 98, no. 12, 2005, Art. no. 124903.
[30] J. J. Dittmer et al., "Crystal network formation in organic solar cells," *Sol. Energy Mater. Sol. Cells*, vol. 61, no. 1, pp. 53–61, 2000.
[31] G. Wei et al., "Efficient, ordered bulk heterojunction nanocrystalline solar cells by annealing of ultrathin squaraine thin films," *Nano Lett.*, vol. 10, no. 9, pp. 3555–3559, 2010.
[32] M. Biber et al., "The influence of annealing temperature and time on the efficiency of pentacene: PTCDI organic solar cells," *Results Phys.*, vol. 7, pp. 3444–3448, 2017.
[33] L. Y. Lin et al., "A low-energy-gap organic dye for high-performance small-molecule organic solar cells," *J. Amer. Chem. Soc.*, vol. 133, no. 40, pp. 15822–15825, 2011.
[34] Y. H. Chen et al., "Vacuum-deposited small-molecule organic solar cells with high power conversion efficiencies by judicious molecular design and device optimization," *J. Amer. Chem. Soc.*, vol. 134, no. 33, pp. 13616–13623, 2012.
[35] M. A. Faist et al., "Understanding the reduced efficiencies of organic solar cells employing fullerene multiadducts as acceptors," *Adv. Energy Mater.*, vol. 3, no. 6, pp. 744–752, 2013.
[36] Q. Yue et al., "Vacuum-deposited organic solar cells utilizing a low-bandgap non-fullerene acceptor," *J. Mater. Chem. C*, vol. 10, no. 7, pp. 2569–2574, 2022.
[37] H. S. Shim et al., "Efficient vacuum-deposited ternary organic solar cells with broad absorption, energy transfer, and enhanced hole mobility," *ACS Appl. Mater. Interfaces*, vol. 8, no. 2, pp. 1214–1219, 2016.
[38] K. Tvingstedt et al., "Electroluminescence from charge transfer states in polymer solar cells," *J. Amer. Chem. Soc.*, vol. 131, no. 33, pp. 11819–11824, 2009.
[39] A. P. Demchenko, *Introduction to Fluorescence Sensing*. New York, NY, USA: Springer, 2009, pp. 1–586.
[40] J. Min et al., "Gaining further insight into the effects of thermal annealing and solvent vapor annealing on time morphological development and degradation in small molecule solar cells," *J. Mater. Chem. A*, vol. 5, no. 34, pp. 18101–18110, 2017.
[41] B. P. Rand, D. P. Burk, and S. R. Forrest, "Offset energies at organic semiconductor heterojunctions and their influence on the open-circuit voltage of thin-film solar cells," *Phys. Rev. B Condens. Matter Mater. Phys.*, vol. 75, no. 11, pp. 1–11, 2007.
[42] H. Kim, J. Hwa Seo, and S. Cho, "Effect of a symmetry breaking layer on the open circuit voltage of conventional bulk-heterojunction solar cells," *Appl. Phys. Lett.*, vol. 99, no. 21, pp. 2–5, 2011.
[43] C. W. Schlenker and M. E. Thompson, "The molecular nature of photovoltage losses in organic solar cells," *Chem. Commun.*, vol. 47, no. 13, pp. 3702–3716, 2011.
[44] S. S. Hegedus and W. N. Shafarman, "Thin-film solar cells: Device measurements and analysis," *Prog. Photovolt., Res. Appl.*, vol. 12, no. 2/3, pp. 155–176, 2004.
[45] J. Appelbaum and A. Peled, "Parameters extraction of solar cells—A comparative examination of three methods," *Sol. Energy Mater. Sol. Cells*, vol. 122, pp. 164–173, 2014.
[46] S. Yamamoto, A. Orimo, H. Ohkita, H. Benten, and S. Ito, "Molecular understanding of the open-circuit voltage of polymer: Fullerene solar cells," *Adv. Energy Mater.*, vol. 2, no. 2, pp. 229–237, 2012.
[47] G. Long et al., "Investigation of quinquethiophene derivatives with different end groups for high open circuit voltage solar cells," *Adv. Energy Mater.*, vol. 3, no. 5, pp. 639–646, 2013.
[48] L. Yang, H. Zhou, and W. You, "Quantitatively analyzing the influence of side chains on photovoltaic properties of polymer-fullerene solar cells," *J. Phys. Chem. C*, vol. 114, no. 39, pp. 16793–16800, 2010.
[49] P. Schilinsky, C. Waldauf, and C. J. Brabec, "Recombination and loss analysis in polythiophene based bulk heterojunction photodetectors," *Appl. Phys. Lett.*, vol. 81, no. 20, pp. 3885–3887, 2002.
[50] I. Riedel et al., "Effect of temperature and illumination on the electrical characteristics of polymer-fullerene bulk-heterojunction solar cells," *Adv. Funct. Mater.*, vol. 14, no. 1, pp. 38–44, 2004.
[51] S. R. Cowan, A. Roy, and A. J. Heeger, "Recombination in polymer-fullerene bulk heterojunction solar cells," *Phys. Rev. B*, vol. 82, no. 24, 2010, Art. no. 245207.
[52] L. J. A. Koster, V. D. Mihailetchi, R. Ramaker, and P. W. M. Blom, "Light intensity dependence of open-circuit voltage of polymer: Fullerene solar cells," *Appl. Phys. Lett.*, vol. 86, no. 12, 2005, Art. no. 123509.